Journal of Physics: Conference Series **102** (2008) 012025 doi:10.1088/1742-6596/102/1/012025

Experimental verification of a Monte Carlo-based MLC simulation model for IMRT dose calculations in heterogeneous media

N Tyagi[1], **B H Curran, P L Roberson, J M Moran, E Acosta and B A Fraass**
Department of Radiation Oncology, The University of Michigan, Ann Arbor, MI, USA, 48109-0010

E-mail: Currently at University of California, San Diego: ntyagi@ucsd.edu

Abstract. IMRT often requires delivering small fields which may suffer from electronic disequilibrium effects. The presence of heterogeneities, particularly low-density tissues in patients, complicates such situations. In this study, we report on verification of the DPM MC code for IMRT treatment planning in heterogeneous media, using a previously developed model of the Varian 120-leaf MLC. The purpose of this study is twofold: (a) design a comprehensive list of experiments in heterogeneous media for verification of any dose calculation algorithm and (b) verify our MLC model in these heterogeneous type geometries that mimic an actual patient geometry for IMRT treatment. The measurements have been done using an IMRT head and neck phantom (CIRS phantom) and slab phantom geometries. Verification of the MLC model has been carried out using point doses measured with an A14 slim line (SL) ion chamber inside a tissue-equivalent and a bone-equivalent material using the CIRS phantom. Planar doses using lung and bone equivalent slabs have been measured and compared using EDR films (Kodak, Rochester, NY).

1. Introduction

Dose calculations for MLC-based IMRT planning are quite challenging primarily because IMRT beams consist of a large number of small segments which may suffer from electronic disequilibrium. In addition, for a complex intensity pattern the dose distributions can be very sensitive to the detailed structure of the multileaf collimator (MLC).[1] The presence of an inhomogeneity exacerbates the existing electronic disequilibrium. The existing literature contains many studies showing the superior performance of Monte Carlo methods in heterogeneous media,[2-7] especially at tissue interfaces.[8-11] Most of these verification studies are, however, limited to conformal beam planning in the presence of inhomogeneities. In this article, we report on verification of the DPM MC code [12] for IMRT treatment planning in heterogeneous media using a previously developed model of the Varian 120-leaf MLC (Varian Medical Systems, Palo Alto, CA).[13] The accuracy of the model has been verified previously against ion chamber and film measurements for several SMLC and DMLC–based IMRT treatment plans in a homogeneous Solid Water phantom.[13] We now compare our MLC model in heterogeneous media using an IMRT head and neck phantom that represents human head and neck anatomy and consists of interchangeable inserts for tissue equivalent and heterogeneous media. In addition, we have compared film measurements and Monte Carlo simulations at multiple depths

[1] To whom any correspondence should be addressed.

(including interfaces) for slab phantom geometries consisting of lung and bone equivalent slabs embedded within Solid Water for 6 MV IMRT treatment beams. Such verification measurement is necessary to document the accuracy of MC-based dose calculations in anatomical sites such as the lung, head and neck, and prostate where tissue heterogeneities make accurate dose calculation challenging.

2. Methods and Materials

2.1. A Phase-space modeling of the linear accelerator

A Varian 21EX linear accelerator equipped with a 120-leaf (Millennium) multileaf collimator was simulated using the BEAMnrc[14] and DPM MC codes. The details of the treatment head simulation have been described in our previous publication.[13] In our model, the "patient-independent" components (target, primary collimator, flattening filter, ion chamber, and mirror) were simulated once using the BEAMnrc MC code and stored in 4 phase-space (PS) files containing approximately 200 million particles. The PS files were read into the DPM MC code and used for the patient-specific calculations which depend on the MLC, jaws and patient geometry. While multiple photon scattering is accounted for, electrons generated within the jaws and MLC deposit their energy locally.[13]

2.2. Measurement and Phantom set-up

Measurements were made in flat and cylindrical geometries. First, verification measurements were made using a Solid Water (Gammex RMI, Middleton WI) phantom of dimensions 30x30x20 cm^3 at 5 cm depth, 95 cm SSD for a 6 MV photon beam as shown in Figure 1. Kodak EDR2 (Extended Dose Range) film were placed at various depths in the phantom. Lung-ICRU (ρ = 0.26 g/cm^3) and Cortical bone (ρ = 1.85 g/cm^3) slab inhomogeneities of thickness 6 cm were placed 4 cm from the top of the phantom. All the processed films were digitized using a laser film digitizer (Lumisys Lumiscan LS75, Kodak, Rochester, NY) and analyzed using a software analysis package, IGOR pro (Interactive Graphics Oriented Research) that reads the Lumisys file formats. The film measurements were taken at the following depths: 3 cm, 4 cm (water/lung or water/bone interface), 8 cm (within the inhomogeneity), 10 cm (lung/water or bone/water interface), and 15 cm (within Solid Water) as illustrated in Figure 1. The films were exposed at a dose rate of 400 MU/min. The IMRT treatment plan sequenced using a partial breast irradiation protocol (intensity pattern shown in Figure 1) was delivered using SMLC (222 segments, 345 MUs and field size = 5x8 cm^2) and DMLC (150 segments and 375 MUs). A dose calibration curve was measured at the same time and used to convert the film response from optical density to dose. In addition, dose differences between calculations and measurements were analyzed using a dose-gradient analysis tool or a gradient compensation method [15] that evaluates local dose differences as a function of the dose gradient at each point in the dose distribution. In gradient compensation method a distance parameter, which is typically the size of the geometric uncertainty (1mm in all our examples), was chosen and the dose differences that might have been caused by this geometric shift were removed.

Additional measurements were performed using a CIRS head and neck IMRT phantom that represents the human head and neck anatomy as a cylindrical geometry. The cylindrical phantom, shown in Figure 2, is 16 cm in diameter and 16 cm in height and allows interchangeable rod/inserts of tissue equivalent and inhomogeneity material. Each insert is 2.5 cm in diameter and can be placed at any of the 5 locations as shown in Figure 2. The phantom includes measurement plugs for point dose measurements using ion chamber, TLDs, diodes, and other small detectors. The phantom also permits the use of film and gel dosimetry, however, their use was not investigated here. The head and neck phantom, with the chamber in position, was scanned using a GE Lightspeed 4 slice CT scanner in various configurations. Helical scans were obtained using a 1.25 mm slice thickness. The scans were transferred to our in-house planning system (UMPLAN), and contours were drawn for the external phantom and chamber volumes for 3-D dose calculation.

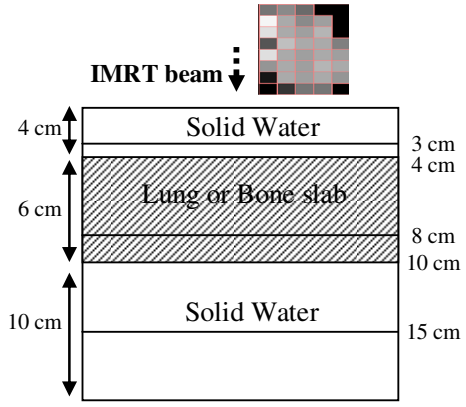

Figure 1.Slab Phantom geometry. Intensity pattern of the incident IMRT beam is also shown.

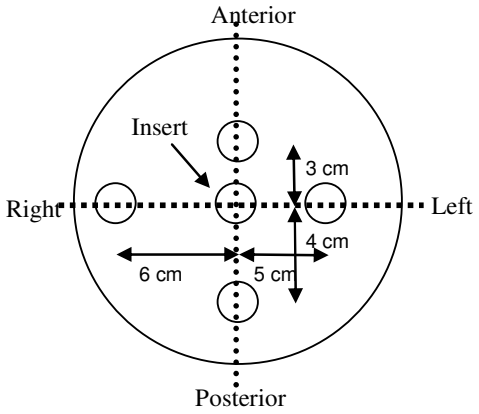

Figure 2. IMRT Head and Neck Phantom consisting of 5 interchangeable inserts for tissue-equivalent and inhomogeneity material.

In this study we have used an A14 SL ion chamber with an active volume of 0.009 cm^3 for point dose measurements. The collected charge was read using an Inovision 35040 electrometer (Standard Imaging). Tissue equivalent, bone equivalent (ρ = 1.6g/cm^3) and air (no insert, ρ = 1.203e-03 g/cm^3) inserts were placed in different locations and with different beam arrangements as described in Table 1. Plans were generated using a 6 MV photon beam in the anterior-posterior (AP) and left-right (LR) direction (IEC gantry angle = 90º) using a 3x3 cm^2 square field formed by jaws and MLC. In addition, the IMRT treatment plan described in the previous section was also delivered using SMLC and DMLC delivery techniques. The isocenter for each plan was assumed to be at the center of the chamber. Each beam was delivered using 200 MU and a dose rate of 600 MU/min for each set-up. Absolute dose calibration was performed by referencing all readings to our standard calibration geometry (SAD = 100 cm, depth = 10 cm, and a 10 x 10 cm^2 field size) in a water phantom. Measured point doses were converted to absolute doses and compared with the MC simulations performed using the DPM MC code.

Table 1. Ion chamber (IC) placement and beam arrangement for the CIRS head & neck phantom.

Case #	IC placement	Isocenter location	SSD (cm)	Beam angles (degrees)
1	Inside Tissue	Origin	92.2	0
2	Inside Tissue	Origin	92.2	90
3	Inside Tissue	2.9 cm Anterior	95.1	0
4	Inside Tissue	5.1 cm Posterior	87.1	0
5	Inside Bone	Origin	92.2	0
6	Inside Bone	2.9 cm Anterior	95.2	0
7	Inside Bone	5.1 cm Posterior	87.1	0
8	Inside Tissue (bone to the left)	Origin	92.2	90
9	Inside Tissue (air to the left)	Origin	92.2	90
10	Inside Tissue (bone to the left and air at the center)	6 cm right	86.1	90

2.3. Monte Carlo Simulations

The DPM MC code, integrated with UMPLAN, was used to calculate dose in CT-based geometries for clinical-like situations. Six different materials (air, lung, adipose tissue, water, muscle and bone) were identified and the corresponding cross-sections were generated. DPM calculations were performed

with a maximum electron condensed history step size of 1 mm and low energy electron and photon cutoffs of 200 keV and 50 keV, respectively. All calculations are reported in absolute dose (cGy) as described in our previous publication. [13] The slab phantom geometry was simulated outside the planning system using the DPM MC code and a voxel size 2x2x1 mm^3. Sufficient histories (~10-20 billion) were simulated for each run such that the uncertainty (1σ) in the average dose over all voxels greater than $Dose_{max}/2$ was less than 1 %. The comparison between calculated and measured doses in heterogeneous media was performed using point-dose comparisons for head and neck phantom geometry and 2-D dose difference maps, gradient compensated dose difference maps and 1-D line profiles at various depths for the slab phantom geometry. In addition issues related to dose reporting by Monte Carlo calculations and film measurements are also discussed. MC reports dose to medium whereas, the film is calibrated with respect to dose to water and is subsequently used to measure doses in different density material. The effect due to discrepancy in dose reporting has been addressed in the future sections.

3. Results and Discussion

3.1 Slab Phantom set-up:

The IMRT beam was delivered using SMLC in the heterogeneous lung phantom. Figures 3 (a)–(e) show the dose difference maps (top graphs) between film measurements and MC calculations (DPM-Film) at depths of 3 cm (within the Solid Water), 4 cm (water/lung interface), 8 cm (within the inhomogeneity), 10 cm (lung/water interface), and 15 cm (within Solid Water) respectively. The middle graphs show the corresponding gradient compensated dose difference maps at these depths and the bottom graphs show the 1-D profiles along the lines shown on the dose difference map for the corresponding dose maps at the same depths. The film data is represented using solid lines and the MC calculation is shown as dashed lines in the 1-D line profiles. The dose difference map shows differences of up to 30-40 cGy, located primarily in the penumbral regions. One possible reason for these differences is the much larger voxel size resolution of the DPM calculation (2 mm) as compared with film (0.1 mm) which could lead to averaging errors in the high dose gradient regions. In the penumbral region, shifts of 1 mm can result in dose differences of 10-20%. When a gradient compensation of 1 mm is applied, many regions of large dose difference disappear. In the out-of-field regions for the IMRT beams, the film over-responds due to its energy response to low-energy scattered photons.[16]

Overall, the film dose is initially higher than MC up until the distal inhomogeneity interface and lower than MC below that depth. The gradient compensated dose difference maps (middle row) represent the differences due to limitations in the MC model or film measurement error. The differences between film and MC (DPM-film) at 3 cm (~ -6 cGy), 4 cm (~ -6 cGy) and 8 cm (~ -3 cGy) depths are within 2 to 3%. The scatter from the MLC mostly consists of low energy photons which may result in an over-response in the film measurements above the inhomogeneity. At the distal interface (10 cm), differences of the order of -3 cGy are seen once again. At a depth of 15 cm inside water, differences of the order of 2.5% (~ (3-4) cGy) are seen between film and MC. The presence of low density media causes a decrease in beam attenuation, changes in photon scatter, and an increased lateral electron range for small fields. The differences seen at lower depths could be due to a variety of factors such as: measurement uncertainties in the positioning of the film (~1 mm), energy response of the film (~2%), uncertainties in film processing (~2%), MC statistical uncertainties (~1%) and uncertainties in the model selection parameters such as the mean electron-on-target energy.

The SMLC-sequenced beam (from the IMRT breast plan) was delivered in a bone equivalent medium as shown in Figures 4 (a)-(e). At depths of 3 cm and 15 cm in water and at the water-bone and bone-water interface (4 cm and 10 cm), the agreement between calculation and film measurement is within 2% with a maximum local difference of 4%. The DPM MC accurately accounts for the backscattered electrons from the bone medium at the proximal interface. Systematic differences of the order of 3.5% were seen between calculation and measurement at 8 cm depth (within the bone

medium). A possible reason for the discrepancy was the medium in which dose is reported: film is calibrated with respect to water and hence reports dose to water where as MC calculation in bone reports dose to the bone. To illustrate this effect a thin layer of water (1mm) was inserted inside the bone medium from 8 cm to 8.1 cm and MC simulations were performed. The dose was evaluated at the depth of 8.05 cm (center of the voxel in z-direction) and the results are shown in Figure 5. The dose difference map, gradient compensated map and profiles now show excellent agreement between measurement and calculation. The 3.5% difference represents the correction that one needs to perform in converting dose-to-medium to dose-to-water or vice versa. This difference, especially significant for high Z material, arises from the difference in stopping power of the electron spectrum in the two media. This difference, is however, not consistent with the stopping power ratios (~10-12%) reported by Siebers *et al* for the cortical bone and is quite puzzling.[17] At this point we do not have a clear explanation for this discrepancy. We are still investigating this issue.

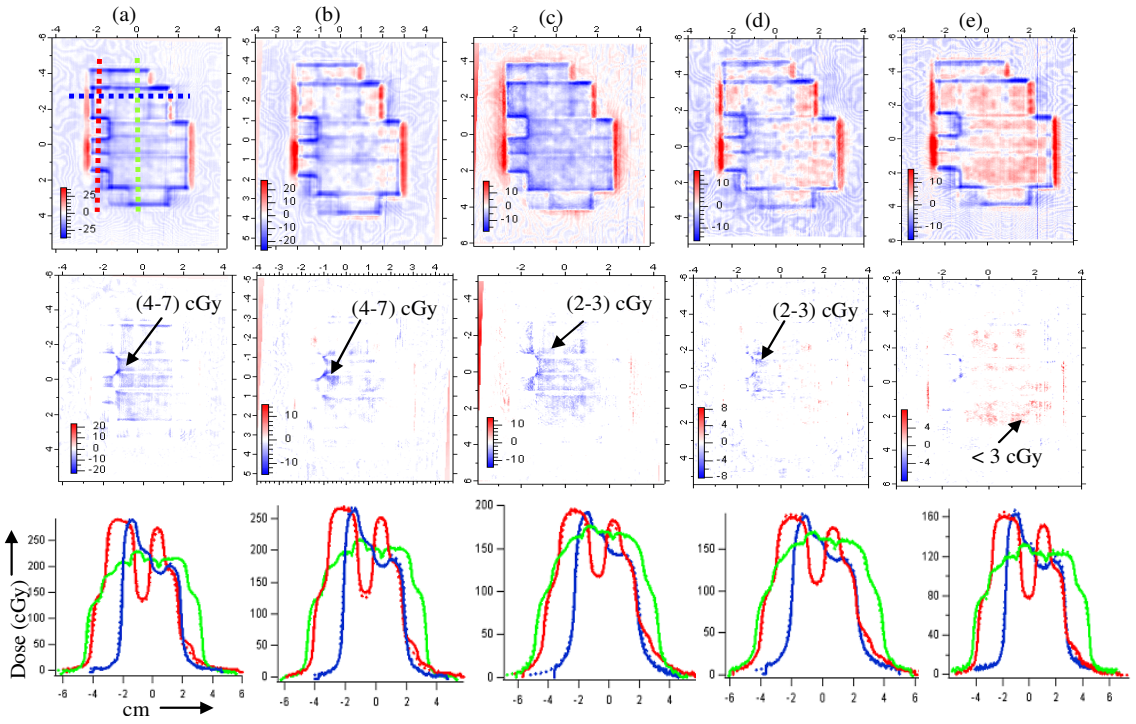

Figure 3: IMRT beam simulated using SMLC delivered in a lung slab medium (ρ = 0.26 g/cm3) Dose difference map (DPM-film), Gradient compensated dose difference map and 1-D profiles (along the lines shown on the dose difference map) at depths of (a) 3 cm (b) 4 cm(c) 8 cm (d) 10 cm and (e) 15 cm. Profile comparisons between film and MC; film is shown in solid and MC in dashed lines at depths of (a) 3 cm (b) 4 cm (c) 8 cm (d) 10 cm and (e) 15 cm.

3.2. IMRT Head and Neck set-up

Table 2 shows the absolute dose comparison between measured data and DPM MC calculations for various situations described in Table 1. All the comparisons on an average are within 2% of the measured data. Cases 1-4 represent the situation where ion chamber was placed inside a tissue equivalent medium at various SSDs and different gantry angles. The agreement between measurement and simulations is excellent. For the situation where ion chamber is placed inside bone at various SSDs (cases 5,6 and 7) slightly higher discrepancies are seen. The differences are within the combined statistical uncertainty associated with MC simulations and measurements. As reported by Bouchard *et*

al, the reference calibration is not valid for IMRT fields or presence of inhomogeneities due to lateral disequilibrium effect that may affect the chamber fluence correction factor. [18] For a dynamic IMRT field the correction factors could be as high as 10% and requires a field dependent correction factor. In addition, ion chamber is reporting dose-to-water in bone and like film would require a stopping power correction which is not very significant in the situation (< 2%) as the beam passes through only 1.25 cm radius of bone. Also, the center of the measurement plug inside the bone insert was found to be off by 2 mm during the scans. Although the position of the chamber was marked on the bone insert after the scan, a slight difference in set-up error may account for slight differences.

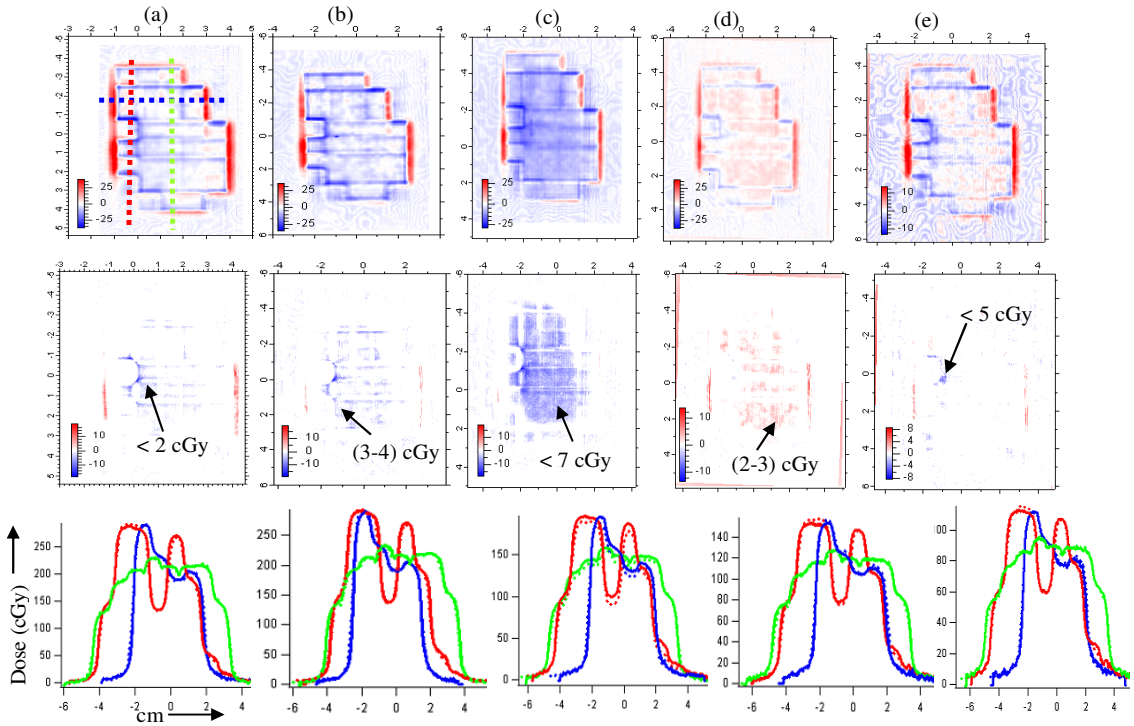

Figure 4. IMRT beam simulated using SMLC delivered in a bone slab medium (ρ = 1.85 g/cm3) Dose difference map (DPM-film), Gradient compensated dose difference map and 1-D profiles (along the lines shown on the dose difference map) at depths of (a) 3 cm (b) 4 cm(c) 8 cm (d) 10 cm and (e) 15 cm. Profile comparisons between film and MC; film is shown in solid and MC in dashed lines at depths of (a) 3 cm (b) 4 cm (c) 8 cm (d) 10 cm and (e) 15 cm.

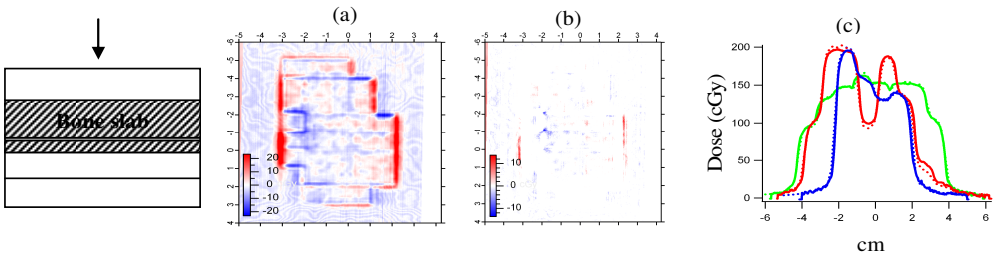

Figure5. Effect of reporting dose-to-water in a bone medium. Simulation carried out by inserting a 1mm layer of water (from 8 - 8.1 cm) in a bone equivalent medium. (a) Dose difference map (DPM-film) (b) Gradient compensated dose difference map and 1-D line profiles at the depth of 8 cm.

When the beam passes through a 2.5 cm of high density bone (case # 8) it results in roughly a 5% reduction in dose to the ion chamber at the center (compared to the homogeneous situation) while the presence of air (case #9) enhances the dose to the chamber by approximately 10%. As shown in Table 2, DPM simulations accurately accounts for these effects.

A single beam in the AP direction from a breast IMRT plan was delivered using SMLC and DMLC delivery techniques. The results are shown in Table 3. The ion chamber was located at the center of the phantom inside a tissue equivalent and bone equivalent medium. The main purpose of this test was to investigate the sensitivity of IMRT beams to the curvature/contour of the phantom. The difference between ion chamber measurements and DPM MC calculations is 2% or less in both homogeneous and heterogeneous medium. The IMRT ion chamber measurements are very sensitive to the chamber position within the phantom and require a field dependent correction factor.[18] The differences are within measurement and calculation uncertainty.

Table 2. Absolute dose comparison between IC measurement and DPM MC calculation for the IMRT head and neck phantom set-up. A 6MV, 3x3 cm^2 beam was delivered to the phantom.

Case #	IC placement	Measured Data (cGy)	Monte Carlo (cGy)	% difference $(\frac{IC-MC}{IC})x100$
1	Inside Tissue	72.33	72.43	-0.1
2	Inside Tissue	73.04	72.40	0.9
3	Inside Tissue	83.09	82.19	1.1
4	Inside Tissue	57.47	58.02	-1.0
5	Inside Bone	72.22	73.68	-2.0
6	Inside Bone	82.51	83.68	-1.4
7	Inside Bone	57.64	56.50	2.0
8	Inside Tissue (bone to the left)	68.76	68.52	0.4
9	Inside Tissue (air to the left)	80.4	80.3	0.1
10	Inside Tissue (bone to the left and air at the center)	57.74	57.89	-0.3

Table 3. Absolute dose comparison between IC measurement and DPM MC calculation for the IMRT head and neck phantom. A 6MV, IMRT beam was delivered to the phantom.

Case #	IC placement	Measured Data (cGy)	Monte Carlo (cGy)	% difference $(\frac{IC-MC}{IC})x100$
SMLC	Inside Tissue	179.43	176.75	1.5
DMLC	Inside Tissue	181.59	183.75	-1.2
SMLC	Inside Bone	176.22	176.45	-0.2
DMLC	Inside Bone	177.4	180.55	-2.0

4. Discussion and Conclusions

In this study we have verified a previously developed model of a 120-leaf MLC (Varian 21 EX) within the DPM Monte Carlo code using ion chamber and film measurements in phantoms with high and low density inhomogeneities for square and IMRT fields. Lung and bone simulations in a slab phantom geometry show excellent agreement between film measurements and calculations. Bone simulations raise an important concern regarding reporting dose to water or to the medium. Measurement dosimetry (film, ion chamber or TLDs) is typically based on dose-to-water. Commissioning and verification of a dose calculation algorithm, especially MC-based thus requires a good understanding of measurement dosimetry and care must be taken to convert the simulated dose in the medium to dose

to water. MC simulations can thus potentially be used to calculate these correction factors as they depend on the beam energy and the measurement set-up. The agreement between ion chamber measurements and DPM MC calculations using a cylindrical head and neck phantom (CIRS) at varying SSDs is excellent when the chamber is placed inside a tissue equivalent or a high density bone inhomogeneity. In addition to the simulations, errors also lie in the manufacturing of the head and neck phantom and measurement plugs inside the inserts. The CT scans showed a shift in the measurement plug inside the bone insert and also a small amount of air in between the inserts and the chamber due to imperfections in the manufacturing of these rods. IMRT simulations carried out in the head and neck phantom geometry show good agreement between measurement and calculation when the chamber was placed at the center of the phantom inside a homogenous and bone equivalent medium. Such verification experiments are important to document the accuracy of any dose calculation algorithm in realistic patient-type geometry. A well benchmarked MC code in homogeneous and heterogeneous geometry provides an alternative QA tool by allowing dose calculation in full 3-D patient geometry. It also enables us to do a retrospective analysis of patients previously treated using IMRT on various protocols to investigate the effect of an improved dose calculation algorithm on clinical outcomes.

Acknowledgements
This work is supported by NIH grant: P01CA59872. The authors would like to thank Dr. Indrin Chetty for extremely useful comments on the paper. Thanks to Brian Tollenaar and Maria Dittman for their assistance in scanning the CIRS phantom.

References
[1] R. Mohan, M. Arnfield, S. Tong, Q. Wu, and J. Siebers, *Med. Phys.* **27** (6), 1226-37 (2000).
[2] C. Martens, N. Reynaert, C. De Wagter, P. Nilsson, M. Coghe, H. Palmans, H. Thierens, and W. De Neve, *Med. Phys.* **29** (7), 1528-35 (2002).
[3] W. U. Laub, A. Bakai, and F. Nusslin, *Phys. Med. Biol.* **46** (6), 1695-706 (2001).
[4] F. C. du Plessis, C. A. Willemse, M. G. Lotter, and L. Goedhals, *Med. Phys.* **28** (4), 582-9 (2001).
[5] M. Miften, M. Wiesmeyer, A. Kapur, and C. M. Ma, *J Appl. Clin. Med. Phys.* **2** (1), 21-31 (2001).
[6] J. Seco, E. Adams, M. Bidmead, M. Partridge, and F. Verhaegen, *Phys.Med. Biol.* **50** (5), 817-30 (2005).
[7] J. J. DeMarco, T. D. Solberg, and J. B. Smathers, *Med. Phys.* **25** (1), 1-11 (1998).
[8] S. N. Rustgi, A. K. Rustgi, S. B. Jiang, and K. M. Ayyangar, *Phys. Med. Biol.* **43** (12), 3509-18 (1998).
[9] O. Chibani and X. A. Li, *Med. Phys.* **29** (5), 835-47 (2002).
[10] E. E. Klein, L. M. Chin, R. K. Rice, and B. J. Mijnheer, *Int. J. of Radiat. Oncol. Biol. Phys*. **27** (2), 419-27 (1993).
[11] K. R. Shortt, C. K. Ross, A. F. Bielajew, and D. W. O. Rogers, *Phys.Med.Biol.* **31** (3), 235-49 (1986).
[12] J. Sempau, S. J. Wilderman, and A. F. Bielajew, *Phys. Med. Biol.* **45** (8), 2263-91 (2000).
[13] N. Tyagi, J. Moran, D. Litzenberg, A. Bielajew, B. Fraass, and I. Chetty, *Med Phys* **34**, pp 651-663 (2007).
[14] D.W.O. Rogers, B. Walters, and I. Kawrakow, BEAMnrc Users Manual: NRC Report PIRS 509(a)revH. (2004).
[15] J. M. Moran, J. Radawski, and B. A. Fraass, J. Appl. Clin. *Med. Phys*. **6** (2), 62-73 (2005).
[16] P. J. Muench, A. S. Meigooni, R. Nath, and W. L. McLaughlin, *Med. Phys.* **18** (4), 769-75 (1991).
[17] J. V. Siebers, P J Keall, A E Nahum and R Mohan, *Phys. Med. Biol.* **45** (4), 983-995 (2000).
[18] H. Bouchard and J. Seuntjens, *Med. Phys.* **31** (9), 2454-2465 (2004).